

# GAMMA Portable Radar Interferometer GPRI



Figure 1: GPRI during observation of a slope instability at Matterhorn, Switzerland.

## 1. Introduction

The GAMMA Portable Radar Interferometer (GPRI) is a ground-based real-aperture radar system working at Ku-band with 17.2 GHz. It is ideally suited for millimeter-precision deformation measurements, long-term monitoring, and digital elevation model (DEM) generation. A high signal quality within up to 10 km radius is ensured by the high gain of the real-aperture antennas. A full 360° area can be monitored by the rotating antennas. The system can be deployed rapidly and provides very high temporal resolution. The standard GPRI supports interferometric repeat-pass and single-pass acquisitions. For advanced studies, GAMMA manufactures polarimetric and polarimetric-interferometric GPRI as well as a bistatic version with two synchronized GPRI.

A wide range of applications and dynamic processes is covered by different operation modes. Observable processes are, e.g., flexure of bridges, vibration of infrastructure, motion of sea ice, ocean waves, snow avalanches, landslides, glacier flow, slope stability assessment, movements of infrastructure, surface deformation due to underground working or mining, DEM generation and volume change measurements on natural mass movements and mining.

GAMMA developed and built the GPRI and uses it regularly for its own research activities and services. We are dedicated to keep the GPRI instrument, related optional elements, and the GAMMA processing software at a very advanced level.

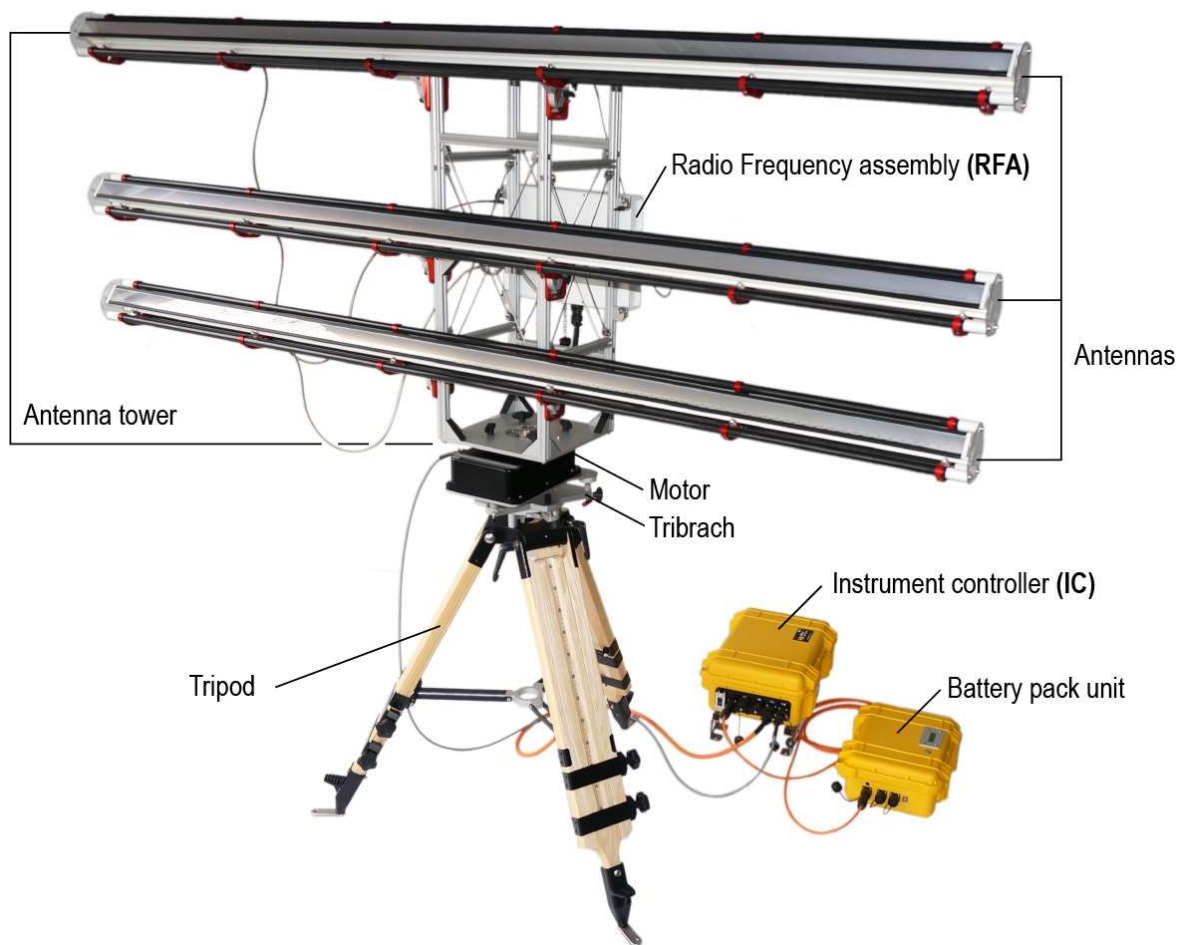


Figure 2: The Standard GPRI.

## 2. Instrument Types

	Standard GPRI	GPRI with additional H-pol. antenna	Polarimetric GPRI
Frequency	17.2 GHz	17.2 GHz	17.2 GHz
Chirp bandwidth	200 MHz	200 MHz	200 MHz
Transmit/receive channels	1 / 2	1 / 2	2 / 4
V-pol. / H-pol. antennas	3 / 0	3 / 1	3 / 3
Radome option	x	x	x
Continuous mode	x	x	x
Revisit mode	x	x	x
Staring mode	x	x	x
Topography mode	x	x	x
Backscatter & coherence	x	x	x
Dual-pol. (VV, VH)		x	x
Fully polarimetric			x

## Standard GPRI

The standard GPRI comes with one transmit and two receive antennas (all vertically polarized). The two-meter-long antennas result in a very narrow beam ( $0.4^\circ$ ). They have a high gain and very low sidelobe levels. Due to the gain and beam pattern, a very high signal quality is achieved, permitting interferometric measurements for distances  $> 10$  km. The two receive antennas, separated by a vertical baseline, support topographic and volume measurements. Having two separate receivers also reduces the probability of failures – a relevant advantage in monitoring applications. Measurements can cover large angular sectors up to a full  $360^\circ$  view.

The GPRI is portable and can be transported in standard cars and in helicopters. Rapid deployment in less than 30 minutes allows for disaster monitoring and efficient measurement campaigns. Besides operation in the continuous mode, we often use it in the revisit mode to monitor slower movements. At least one millimeter of line-of-sight displacement is required to have a reliable indication of movement. As an example, measuring in a revisit mode of twice a year is a reasonable approach to monitor a rock wall with sections showing a displacement rate of 3 mm/year. Further applications cover DEM generation, backscatter measurements, coherence analysis, etc.

External power supply, tripod, shipping containers and an antenna bag are included.

## Standard GPRI with an additional H-polarized antenna

With one additional H-polarized antenna, the standard GPRI can support simultaneous co-/cross-polarized measurements (VV and VH). Adjustable antenna mounts provide a fine adjustment of the pointing direction of the H-pol. antenna to match the pointing of the V-pol. antennas. The second receiver is used for the H-polarized antenna.

## Polarimetric GPRI

The polarimetric GPRI (POL-GPRI) has a 20 cm higher tower than the standard GPRI and comes with three additional H-polarized antennas (one for transmit, two for receive). The radiofrequency assembly includes switching capability to provide two independent transmit channels (V and H) and in total four receive channels to support fully polarimetric-interferometric measurements, alternating-bistatic measurements and more.

## Bistatic GPRI

The GPRI can be modified to synchronize two standard or polarimetric GPRI radar systems via cable or radio connection to acquire bistatic radar data with arbitrary bistatic angles.



Figure 3: The polarimetric GPRI.

### 3. GAMMA Software

The GPRI instrument software (written in Python) supports the operation of the instrument, the data acquisition, and the processing of the raw data to single-look complex (SLC) images.

Further processing steps, such as geocoding, interferometry, atmospheric filtering, phase unwrapping, offset-tracking, time-series analysis, are fully supported by the GAMMA software. The GAMMA software offers a very wide range of functionality and the possibility to automate operational processes. Further information is available on <https://www.gamma-rs.ch/software>.

### 4. GPRI Radome

For long-term monitoring and to provide excellent environmental protection in harsh conditions, a 2.5 m diameter radome with pedestal and a 1.2 m galvanized steel base is available. The radome is designed for winds up to 150 km/h and can be mounted on a concrete pad. Optional extended base supports are available for deployment without a concrete pad. The radome can also be mounted on a trailer or truck for mobile deployment. The radome has low attenuation ( $< 2$  dB) and a constant phase delay. Active ventilation controls the temperature of the radome interior.



Figure 4: GPRI Radome with steel base.

## 5. GPRI Measurement Modes

To observe a large variety of processes with different environmental conditions, the GPRI system can be deployed in multiple different measurement modes.

### Continuous mode

Surface motions of one millimeter to several meters per day can be detected continuously within a single-day campaign over a wide range of terrain types. Continuous long-term monitoring, where the system operates autonomously in the field, can be used for early warning systems and alerting. In the continuous mode, acquisition intervals  $\Delta t$  of minutes to hours allow for monitoring of quickly decorrelating natural surfaces like snow, ice, or vegetation. Rotation of the antennas provides full 360° panoramic scans within less than a minute.

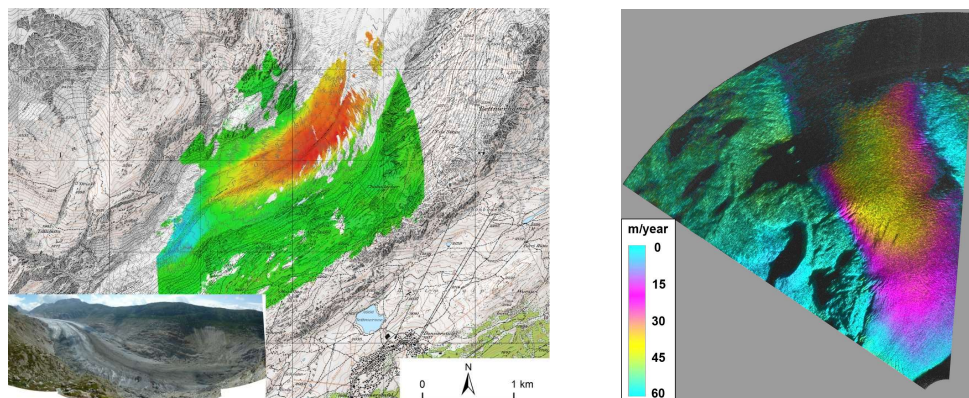


Figure 5: (left) Line-of-sight (LOS) component of **glacier flow velocity** of the Great Aletsch Glacier. Color scale blue / red: -/+30 cm per day [1]. Right: LOS velocity of the Rhone Glacier obtained from four interferograms with  $\Delta t = 80$  minutes. [2]. Further examples of glacier flow are shown in [3]. Observation of sea ice motion up to full 360° view are shown in [4] and [5].

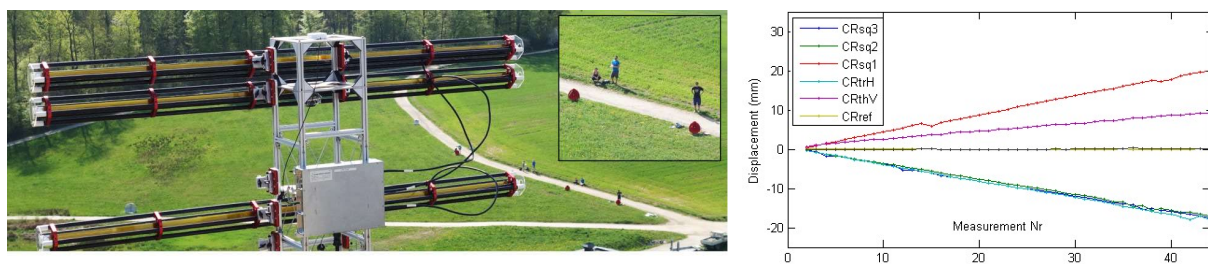


Figure 6: **Displacement of radar reflectors** at ETH Zürich during a radar interferometry course demonstrates sub-mm displacement measurements and **detection of point targets**.

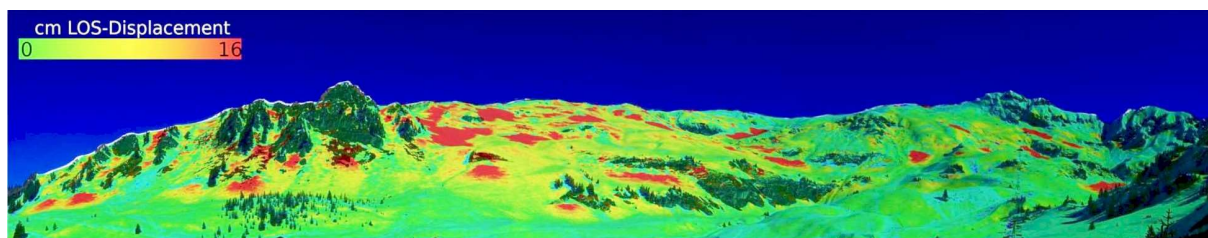


Figure 7: **Displacement of melting snow** during 3 March 2012 ( $\Delta t = 2$  min). Red indicates deformation of 16 cm/day [6]. The panoramic view covers a 160° view angle.

Examples of slope instabilities in different terrain types:



Figure 8: Monitoring of a **slope instability** in the Round Mountain Gold Mine, Nevada, USA, over vegetation-free terrain with an acquisition interval of  $\Delta t = 17$  min.

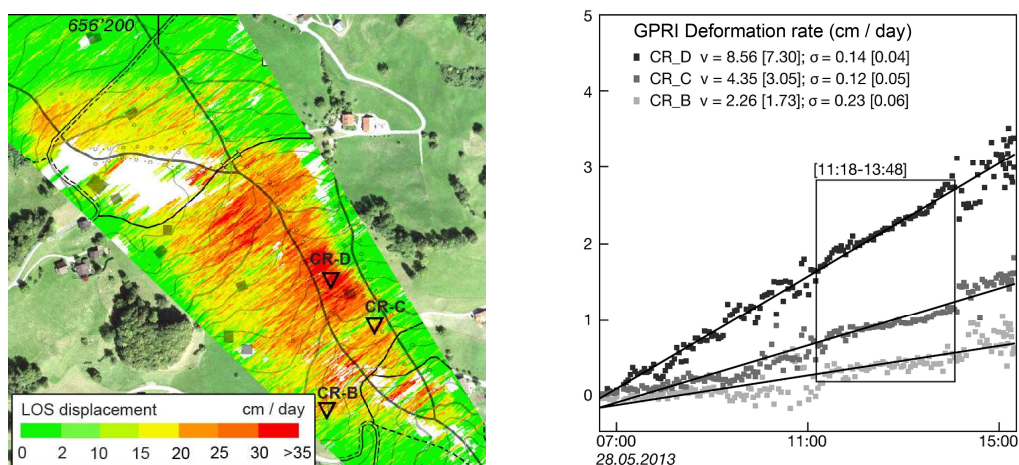


Figure 9: Monitoring of a fast **landslide** in terrain covered by 20 cm high grass. With the fast acquisition interval of the GPRI (here:  $\Delta t = 3$  min), sufficient interferometric coherence is still obtained despite the vegetation cover.

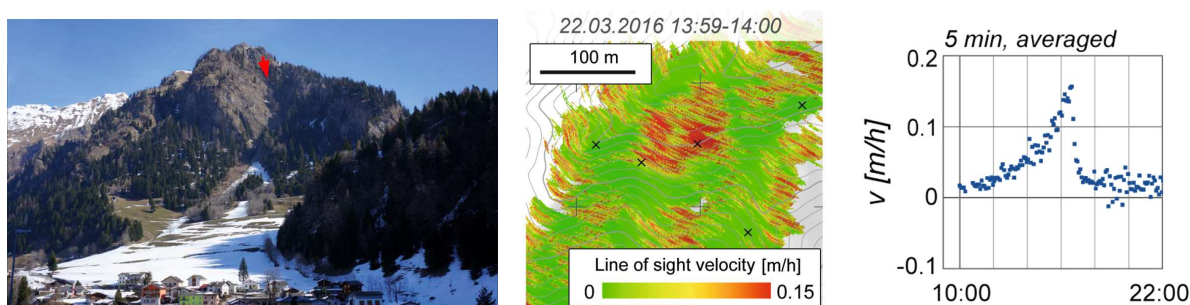


Figure 10: Monitoring of a **landslide** (2016) above the village of Ghirone, Switzerland. After detection of the moving area (middle), time series with  $\Delta t = 1$  min, averaged to 5 min, show a **rapid acceleration** six hours prior to a rockfall event [7].

**Revisit mode**

Very slow movements of millimeters to meters per year can be detected with long-term monitoring using the revisit mode. In this mode, data are acquired by revisiting the same place every few months to years. This mode has the advantage, that multiple sites can be monitored simultaneously over many years. The GPRI can be repositioned precisely to provide consistent data quality.

Examples for monitoring are instabilities of rock slopes, hydropower dams, subsidence of infrastructure, urban environment and buildings.

The requirement, that the radar signal does not decorrelate within several months or years, favors vegetation-free, rock-like surfaces and infrastructure. The GAMMA software supports precise coregistration, phase-correction and filtering of the acquired radar images.

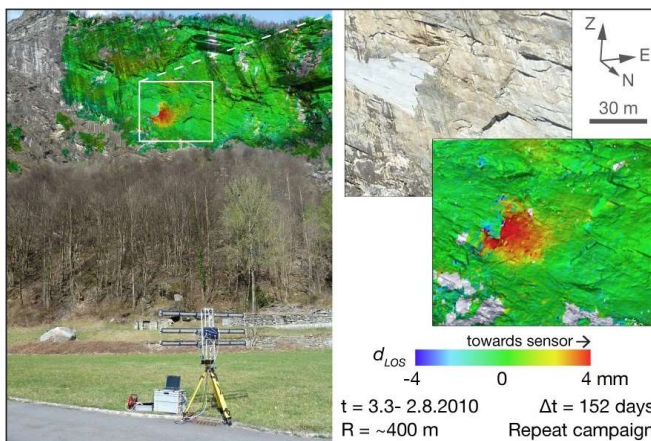


Figure 11: Monitoring of a **rock instability** of 8 mm / year at Soazza, Switzerland with a revisit time of  $\Delta t = 6$  months.

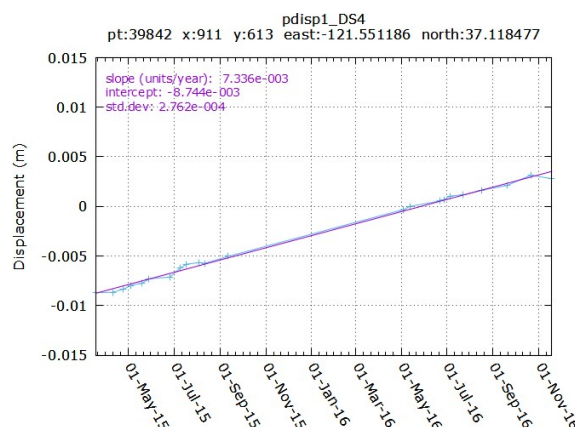


Figure 12: **Stability assessment** of Coyote dam in California. The dam is built on the Calaveras fault zone which moves 1-2 cm / year. Measurements were done every 1-2 weeks over 1.5 years.

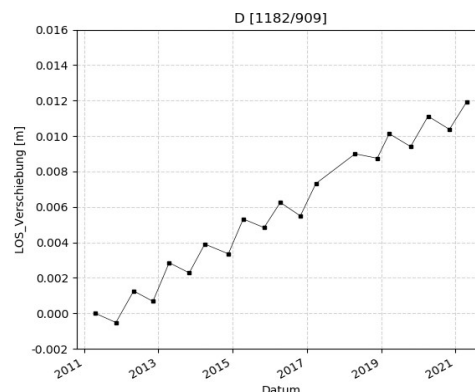
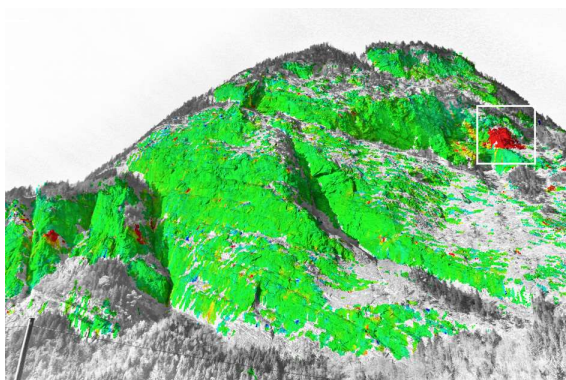


Figure 13: **Long-term monitoring** of rock instabilities by revisiting the same place every six months over **12 years** at a rock face in the Swiss Alps. The linear movement rate is 1.2 mm / year.

### Staring mode

Very fast movements of millimeters to meters per second can be observed in the staring mode. The fast acquisition rate of up to 4 kHz and pulse-to-pulse interferograms from a fixed antenna position (staring) can reveal rapid motion and vibrations.

Application examples are the flexure and vibrations of bridges [8] and the observation of infrastructure and vegetation movement. Fast processes, such as snow avalanches and mud flows, can be characterized. The vibration power spectrum can reveal material damage of dams, towers, bridges, and wind turbines [9].

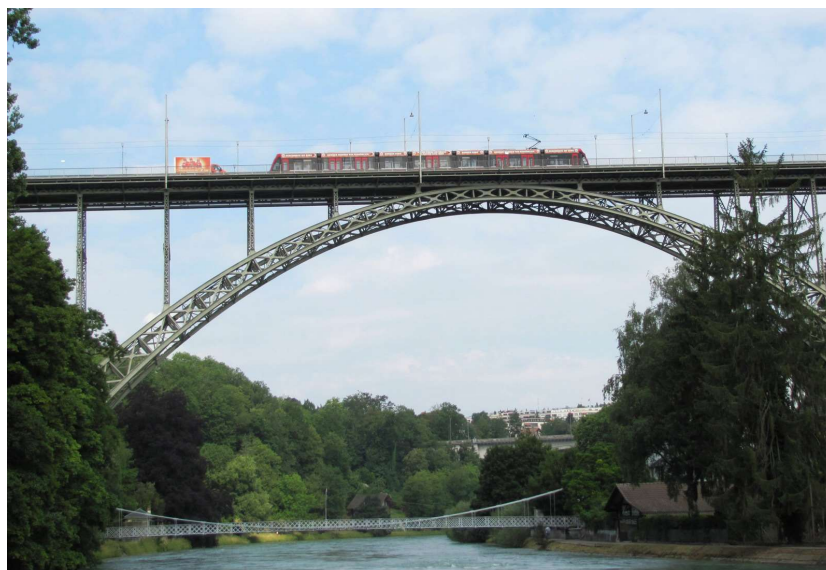


Figure 14: **Flexure of infrastructure** (Kornhausbrücke, Bern) can be measured with a **repeat rate of up to 4 kHz**.

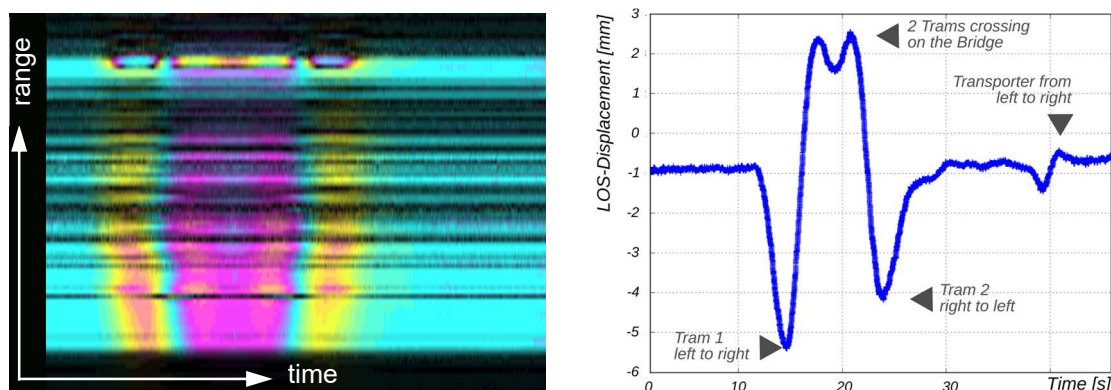


Figure 15: Time series of **pulse-to-pulse interferograms** (left) reveal transient flexure of a bridge (right) during vehicle crossing [10].

## Topography mode

The GPRI has two simultaneously operating receive antennas (single-pass mode). Due to the simultaneous data acquisition, temporal decorrelation cannot reduce the interferometric precision. Furthermore, phase errors due to tropospheric path delays cancel out. With the GAMMA software, a 3-D point cloud can be generated and processed into a digital elevation model (DEM).

Volume change measurements can be calculated from DEMs acquired at different times, independent of coherence loss due to surface decorrelation [11] [12]. The DEM acquisition can be done during annually revisit campaigns of a glacier or in the continuous mode, e.g., to monitor glacier calving volumes [13] [5], or by analysis of pre-/post event data for volume change estimation due to rock fall [7] or landslides.

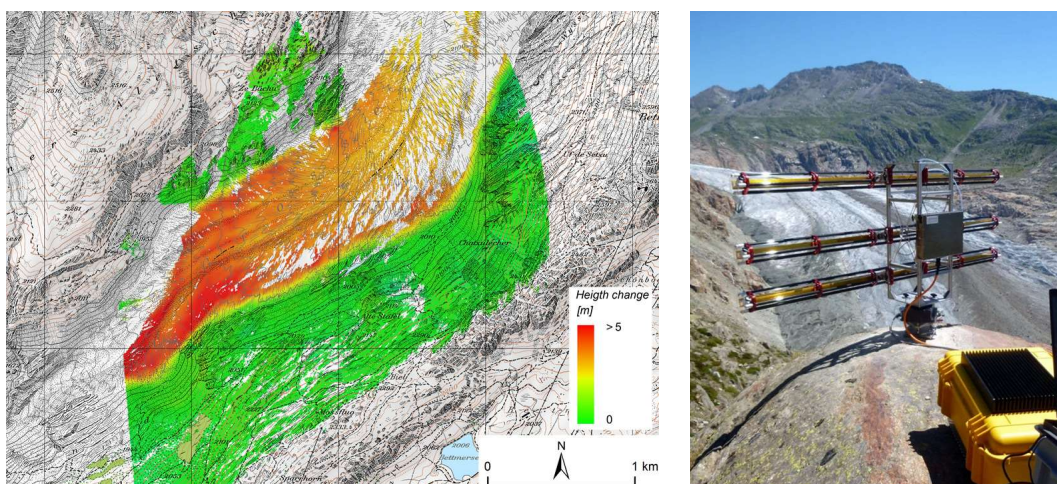


Figure 16: **Height change of Aletsch Glacier** between 27 June and 10 Aug. 2011 indicates >5 m melting.

## POL-GPRI: Additional alternating bistatic mode for DEM generation

Thanks to the two independent transmit channels of the POL-GPRI, an alternating bistatic interferometric mode can be realized through pulse-to-pulse switching of the transmit and receive antennas. This doubles the height sensitivity and the precision of derived DEMs. The image below shows two interferograms: one acquired in the topographic mode of the standard GPRI, and one acquired in the alternating bistatic mode of the POL-GPRI. A doubling of the fringe frequency indicates the increased height accuracy of this mode. For best results, an additional antenna is required, to have in total four antennas at the same polarization.

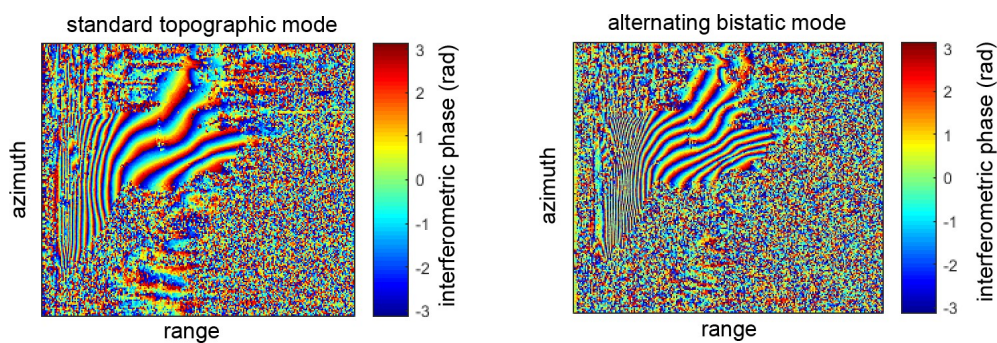


Figure 17: (left) Interferogram in **single-pass mode** of the **standard GPRI**. (right): The interferogram acquired in the **alternating bistatic mode** of the POL-GPRI shows a doubled fringe frequency.

## 6. Backscatter and Coherence Measurements

The analysis of the backscattered intensity and of the temporal coherence provides additional information about the observed scene.

### Monostatic backscatter measurements

The high gain and the low sidelobe of the GPRI antennas enable high-contrast backscatter measurements. Backscatter measurements can be used for land-cover classification, change-detection, detection of persistent scatterers, characterization of radar reflectors, tracking applications, e.g., of ships or sea ice, and for specific polarimetric or bistatic backscatter experiments.

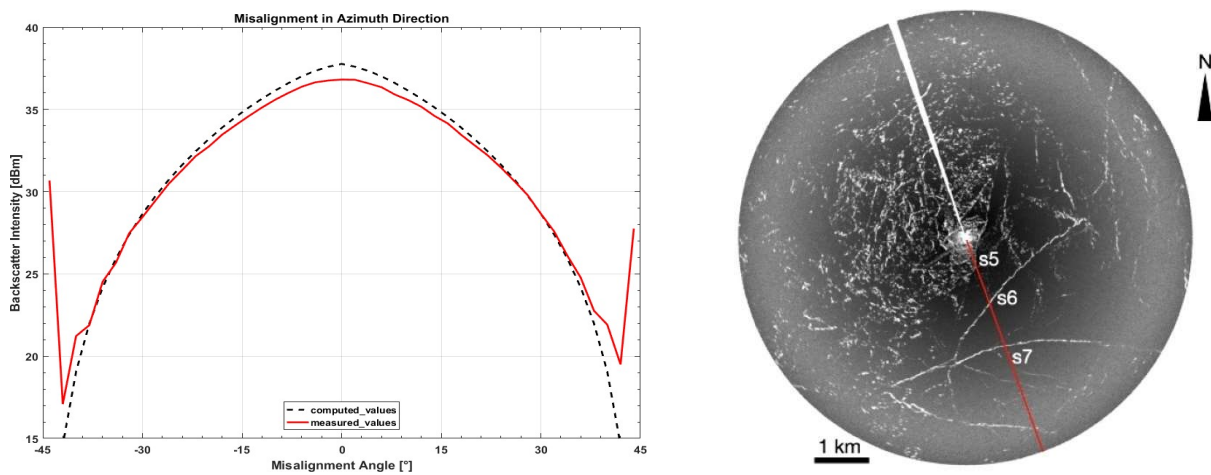


Figure 18: left: **Radar reflector cross section** vs. alignment angle (red: GPRI measurements, black: modelled curve). Right: **Backscatter signal from sea ice** within a 4 km radius [4].

### Bistatic backscatter measurements

Two GPRI systems can be synchronized via cable or radio transmission to transmit at a different position relative to the receive position. With such a setup, bistatic backscatter measurements can be performed to characterize the bistatic reflectance of different objects or surfaces.

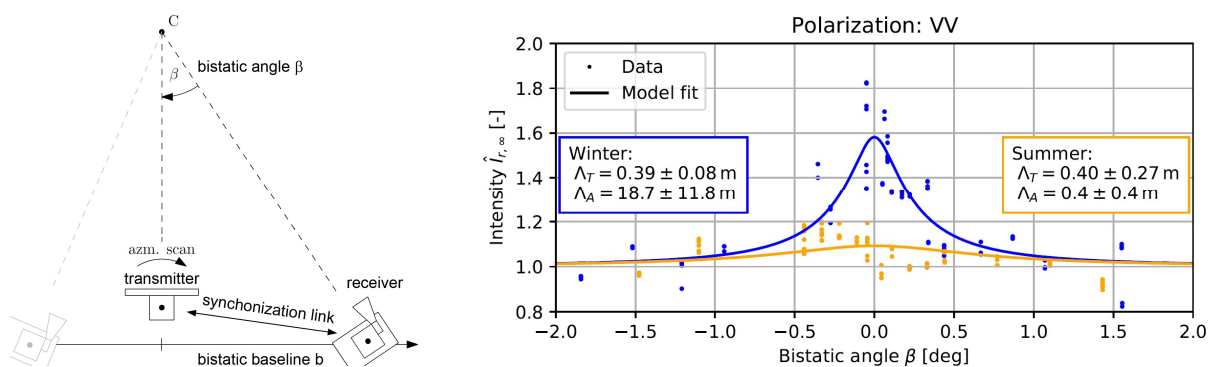


Figure 19: With **bistatic radar backscatter measurements**, coherent backscatter enhancement in dry snow was detected within a very narrow cone of  $0.4^\circ$  around the direct backscatter direction [14].

### Coherence analysis

The analysis of the temporal decorrelation of different surfaces can be used for change detection, surface characterization, as well as to optimize the acquisition interval of certain surfaces.

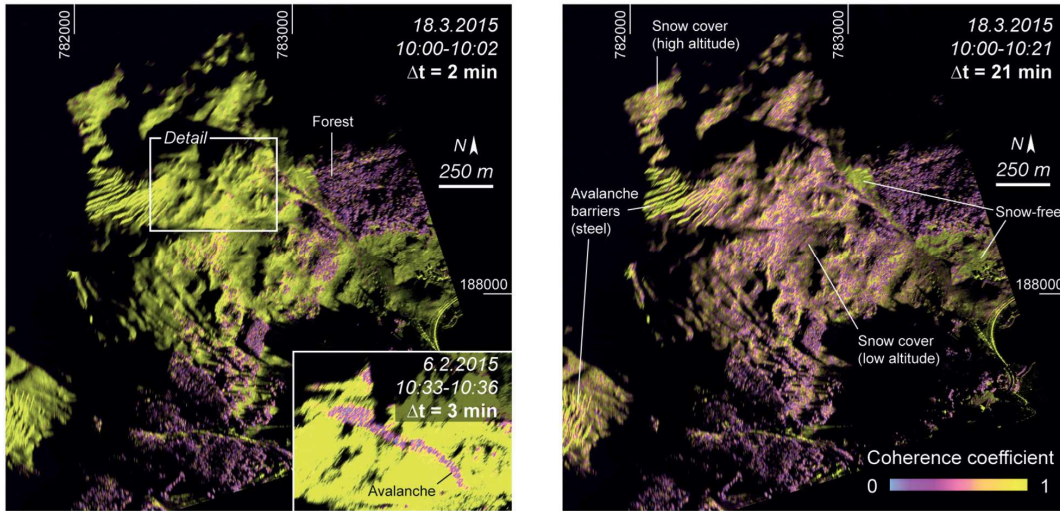


Figure 20: The level of coherence can be used to distinguish between different land cover (here snow and forest) and for change detection (inset: avalanche detection) [15].

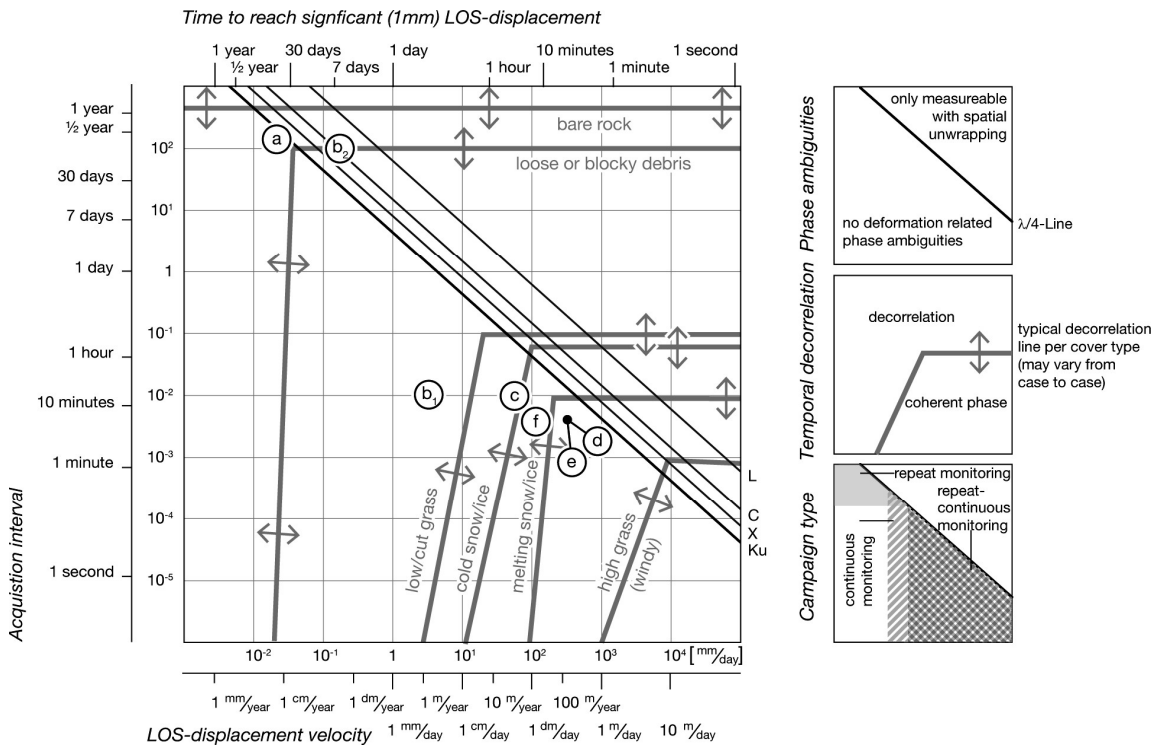


Figure 21: Depending on the interferometric coherence, different acquisition intervals need to be chosen. This plot provides a guideline for the recommended acquisition interval (vertical axis) depending on the expected deformation signal (horizontal axis) and depending on the observed surfaces. Coherence is maintained to the right of and below the grey boundary lines [1].

## 7. Instrument Specification

Table 1: GPRI instrument characteristics (status: 21 Mar. 2022; may change without notice).

Frequency Range and Accuracy	17.1 to 17.3 GHz, 200 MHz bandwidth Frequency accuracy < 100 Hz
Antenna Pattern	0.385 deg -3 dB azimuth beamwidth (2-way) 35 deg -3 dB elevation beamwidth (2-way)
Transmitter Signal Modulation	FM-CW chirp duration: 250 $\mu$ s to 16 ms, 200 MHz max. bandwidth (programmable) POL-GPRI: Transmitter (TX) can switch output ports to A and B
Pulse repetition frequency	50 Hz to 4 kHz
Measurement Range	30 m to >10 km
Time and Frequency Reference	10 and 100 MHz GPS-disciplined crystal oscillator, GPS PPS
Range sample spacing and Resolution	0.75 m sample spacing, 0.95 m -3 dB peak width -26 dB peak range sidelobe
Azimuth Resolution (-3 dB)	6.8m at 1 km range (0.39° beam width), -3 dB peak width -30 dB peak azimuth sidelobe
Deformation Measurement Precision	0.03 mm at 30 dB SNR 0.125 mm at 20 dB SNR
Deformation Measurement Accuracy	Typically, better than 1 mm at 1 km, dependent on water vapor variability
Receiver Channels	Two independent RX channels 14-bit ADC, 6.25 MHz ADC sampling, POL-GPRI: Each receiver (RX1 and RX2) can switch between two input ports, A and B
Power Requirements and Consumption	45 W average, 75 W maximum with 21 - 32 VDC input 50 W average, 80 W maximum with 110 - 240 VAC input
Instrument Computer and OS	Industrial mITX PC, Multi-Core I5 CPU, 16 GB RAM, 1 TB SSD Storage, Ubuntu 20.04 Linux OS, Python 3.8 instrument software
Computer Interfaces	USB2/USB3, 1 Gigabit Ethernet Communication via HTTPS and SSH
Azimuth Scan Rate	Nominal 10 deg/s. Programmable in steps of 0.5 deg/s from 0.5-15 deg/s
Operation Temperature Range	-20 °C to +45 °C (AC power) +50 °C (DC power), able to operate in rain
Instrument Weight (In parentheses for POL-GPRI)	Tower 9.9 kg (11.5 kg), RF Assembly 5.5 kg (6.8 kg), Instrument Computer 5.5 kg, Power supply 4.5/5.8 kg with/without batteries, Antennas 3 x 2.7 kg (H-Pol: 3 x 2.3 kg), Tribrach leveler and azimuth scanner 8.9 kg, Tripod 11 kg
Instrument Dimensions (In parentheses for POL-GPRI)	Tower: 80 x 28 x 28 cm (100 x 28 x 28 cm) RF assembly: 30 x 26 x 6 cm (30 x 26 x 8 cm) Instrument computer: 41 x 33 x 17.5 cm Power supply: 41 x 33 x 17.5 cm Antennas: 210 x 12.5 x 12.5 cm
External power supply / battery:	input: AC (100-240-V AC) and DC (9-36 V DC), output +24 VDC
Batteries (user supply)	21 x Li-Ion Panasonic NCR18650B, 210 Wh, 6A max. current
Conformity	CE (Europe), IC (Canada), FCC (USA)

## 8. Varia

### Maintenance and support

GAMMA uses GPRI instruments for its own research and development activities, which also means that the instrument is kept up to date with the newest developments. Your contacts for the support are those persons who developed the instrument and who use it regularly for their own work.

### Further information

Additional information, e. g., on dates and contents of GAMMA Software training courses, is available at <http://www.gamma-rs.ch>.

To obtain a price list or a specific offer please contact Urs Wegmüller at [wegmuller@gamma-rs.ch](mailto:wegmuller@gamma-rs.ch).

## 9. References

- [1] R. Caduff, F. Schlunegger, A. Kos and A. Wiesmann, "A review of terrestrial radar interferometry for measuring surface change in the geosciences," *Earth surface processes and landforms*, vol. 40, p. 208–228, 2014.
- [2] A. Wiesmann, T. Strozzi and U. Wegmüller, "Measuring deformation and topography with a portable radar interferometer," in *Proc. 13th FIG Symp. Deform. Meas. Anal.*, 2008.
- [3] P. Riesen, T. Strozzi, A. Bauder, A. Wiesmann and M. Funk, "Short-term surface ice motion variations measured with a ground-based portable real aperture radar interferometer," *Journal of Glaciology*, vol. 57, p. 53–60, 2011.
- [4] D. O. Dammann, M. A. Johnson, E. R. Fedders, A. R. Mahoney, C. L. Werner, C. M. Polashenski, F. J. Meyer and J. K. Hutchings, "Ground-Based Radar Interferometry of Sea Ice," *Remote Sensing*, 2021.
- [5] D. Voytenko, *Glaciological Applications of Terrestrial Radar Interferometry*, University of South Florida, 2015.
- [6] A. Wiesmann, R. Caduff and C. Mätzler, "Terrestrial radar observations of dynamic changes in alpine snow," *IEEE Journal of Selected Topics in Applied Earth Observations and Remote Sensing*, vol. 8, p. 3665–3671, 2015.
- [7] R. Caduff and T. Strozzi, "Terrestrial radar interferometry monitoring during a landslide emergency 2016, Ghirone, Switzerland," in *Workshop on world landslide forum*, 2017.
- [8] Y. Zhu, B. Xu, Z. Li, J. Hou and Q. Wang, "Monitoring bridge vibrations based on GBSAR and validation by high-rate GPS measurements," *IEEE Journal of Selected Topics in Applied Earth Observations and Remote Sensing*, vol. 14, pp. 5572–5580, 2021.
- [9] D. Ma, Y. Li, Y. Liu, J. Cai and R. Zhao, "Vibration deformation monitoring of offshore wind turbines based on GBIR," *Journal of Ocean University of China*, vol. 20, p. 501–511, 2021.
- [10] C. Werner, A. Wiesmann, T. Strozzi, A. Kos, R. Caduff and U. Wegmüller, "The GPRI multi-mode differential interferometric radar for ground-based observations," in *EUSAR 2012; 9th European Conference on Synthetic Aperture Radar*, 2012.
- [11] C. Werner, T. Strozzi, A. Wiesmann and U. Wegmüller, "GAMMA's portable radar interferometer," in *Proc. 13th FIG Symp. Deform. Meas. Anal.*, 2008.
- [12] T. Strozzi, C. Werner, A. Wiesmann and U. Wegmüller, "Topography Mapping With a Portable Real-Aperture Radar Interferometer," *IEEE Geoscience and Remote Sensing Letters*, vol. 9, pp. 277–281, 2012.
- [13] A. Walter, M. P. Lüthi and A. Vieli, "Calving event size measurements and statistics of Eqip Sermia, Greenland, from terrestrial radar interferometry," *The Cryosphere*, vol. 14, p. 1051–1066, 2020.
- [14] M. Stefko, S. Leinss, O. Frey and I. Hajnsek, "Coherent backscatter enhancement in bistatic Ku-/X-band radar observations of dry snow," *The Cryosphere Discussions*, vol. 2021, p. 1–32, 2021.
- [15] R. Caduff, A. Wiesmann, Y. Bühler, C. Bieler, P. Limpach and A. G. GAMMA Remote Sensing, "Terrestrial radar interferometry for snow glide activity monitoring and its potential as precursor of wet snow avalanches,"

in *13th Congress Interpraevent 2016: Living with natural risks: 30 May to 2 June 2016, Lucerne, Switzerland. Conference proceedings*, 2016.

- [16] A. Wiesmann and U. Gruner, "Radar-Interferometrie im Einsatz für die Stabilitätsüberwachung von grossflächigen Felswänden," *Swiss Bull. angew. Geol.*, vol. 16, p. 1, 2011.
- [17] T. Strozzi, H. Raetzo, U. Wegmüller, J. Papke, R. Caduff, C. Werner and A. Wiesmann, "Satellite and terrestrial radar interferometry for the measurement of slope deformation," in *Engineering Geology for Society and Territory - Volume 5*, Cham, 2015.
- [18] A. Kos, D. Lunghi, W. Tompkinson, T. Strozzi and A. Wiesmann, "Integration of terrestrial lidar and ground-based radar interferometry for monitoring rock slopes following blast mitigation," in *Geologically active: proceedings of the 11th LAEG Congress, Auckland, New Zealand, 5-10 September 2010*, 2010.
- [19] R. Caduff, A. Kos, F. Schlunegger, B. W. McARDell and A. Wiesmann, "Terrestrial radar interferometric measurement of hillslope deformation and atmospheric disturbances in the Illgraben debris-flow catchment, Switzerland," *IEEE geoscience and remote sensing letters*, vol. 11, p. 434–438, 2013.
- [20] R. Caduff and D. Rieke-Zapp, "Registration and visualisation of deformation maps from terrestrial radar interferometry using photogrammetry and structure from motion," *The Photogrammetric Record*, vol. 29, p. 167–186, 2014.
- [21] R. Caduff, T. Strozzi and A. Wiesmann, "Erfolgreicher Einsatz Terrestrischer Radar-Interferometrie Zur Flächenhaften Vermessung von Ausserordentlichen Hangrutschungsbewegungen Im Gebiet Hintergraben (OW)," *Swiss Bulletin für angewandte Geologie/Swiss Bulletin de géologie appliqué*, vol. 18, p. 129–138, 2013.
- [22] R. Caduff, A. Wiesmann, Y. Bühler and C. Pielmeier, "Continuous monitoring of snowpack displacement at high spatial and temporal resolution with terrestrial radar interferometry," *Geophys. Res. Lett.*, vol. 42, p. 813–820, 2015.